Sequential Extraction, Mobility, and Pollution Loading of Heavy Metals in Soils from the Ikole–Itapaji Area, Southwestern Nigeria.

Adeleke Ojo[1], Olusola Amos Olaolorun[2], and Akinola Oluwatoyin Olagoke[3]

[1, 2 &3]Department of Geology, Faculty of Physical Sciences, Ekiti State University, Ado Ekiti.

DOI: https://doi.org/10.51584/IJRIAS.2026.11060111

Received: 07 June 2026; Accepted: 12 June 2026; Published: 27 June 2026

ABSTRACT

This study investigates the sequential extraction, mobility, and pollution loading of heavy metals in soils from the Ikole–Itapaji area, Southwestern Nigeria. Soil samples collected from seventeen locations were analyzed using a modified seven-step Tessier sequential extraction procedure to partition metals into water-soluble, exchangeable, carbonate-bound, Fe–Mn oxide-bound, organic matter-bound, sulfide/strongly bound, and residual fractions. The objective was to evaluate metal speciation, mobility, and environmental risk using Contamination Factor (CF) and Pollution Load Index (PLI) as complementary pollution indices. Results show that most heavy metals are predominantly concentrated in the residual and Fe–Mn oxide fractions, indicating strong lithogenic control and low overall mobility within the soil system. The carbonate-bound, organic matter-bound, and sulfide fractions also contribute moderately to total metal retention, while the water-soluble and exchangeable phases contain relatively low concentrations, suggesting limited immediate bioavailability under present environmental conditions. However, elevated CF values for Cd and Pb indicate significant enrichment, with Cd reaching severe contamination levels at several sampling locations. The Pollution Load Index reveals that most sites have PLI values greater than 1, indicating overall soil quality deterioration, with pronounced contamination hotspots at SQ3, SQ4, SQ14, and SQ15. These spatial patterns reflect a combination of natural geological background variation and localized anthropogenic inputs. The study concludes that although the geochemical framework of the area is largely dominated by stable lithogenic sources, Cd and Pb represent key environmental concerns. The results highlight the effectiveness of sequential extraction in assessing metal mobility, pollution status, and ecological risk in basement complex terrains.

Keywords: Sequential extraction, Contamination, Anthropogenic input, Basement complex

INTRODUCTION

The distribution and geochemical behaviour of trace metals in soils and sediments have attracted considerable attention because of their environmental significance and relevance to mineral exploration studies. Traditionally, the assessment of metal contamination has relied mainly on total metal concentrations; however, total concentrations alone do not adequately indicate the mobility, bioavailability, or geochemical associations of metals within soils and sediments (Firmino et al., 2025). Consequently, sequential extraction techniques have become widely used for partitioning metals into operationally defined geochemical fractions according to their binding forms. These fractions commonly include water-soluble, exchangeable, carbonate-bound, Fe–Mn oxide-bound, organic matter-bound, sulfide/strongly bound, and residual phases. Among the most commonly applied procedures are the Tessier Sequential Extraction Method and the BCR Sequential Extraction Procedure, both of which have been extensively used in recent geochemical and environmental studies (De Matteis et al., 2023; Ibrahim et al., 2024).

Sequential extraction methods provide valuable information on the mobility, stability, and potential bioavailability of metals in soils and sediments. They also help explain the geochemical processes controlling metal distribution, including adsorption, precipitation, ion exchange, redox reactions, and complexation (Çelebi, 2024). Furthermore, these techniques are useful in distinguishing between lithogenic and anthropogenic sources of metals, thereby improving their application in environmental assessment and mineral exploration studies

(Abule and Ekpete, 2025). Recent studies have shown that metals associated with residual fractions are generally lithogenic in origin and relatively immobile, whereas metals occurring within non-residual fractions such as exchangeable and carbonate-bound phases are more mobile and environmentally available (Firmino et al., 2025). In addition, enrichment of metals within Fe–Mn oxide fractions has been linked to secondary geochemical processes such as weathering and supergene enrichment, which are important in the formation of economically viable mineral deposits (Delina, 2024).

The Ikole–Itapaji area, located within the Nigerian Basement Complex, is underlain by crystalline rocks including gneiss, charnockite, and granitic intrusions that are associated with metallic mineral occurrences. Despite the geological importance of the area, there is limited information on the geochemical fractionation and mobility of heavy metals within the soils. Therefore, this study applies sequential extraction techniques to evaluate the partitioning, mobility, and pollution loading of selected heavy metals in soils from the Ikole–Itapaji area, Southwestern Nigeria.

Description of Study Area

The study area is located within the Ikole–Itapaji axis of Ekiti State in Southwestern Nigeria, forming part of the Precambrian Basement Complex of the West African Craton. It lies approximately between latitudes 7°45′N–8°05′N and longitudes 5°20′E–5°40′E, covering an estimated total surface area of approximately 1,360 km². Encompassing Ikole-Ekiti, Itapaji, and adjoining settlements. The terrain is characterized by undulating topography with elevations ranging from about 300 to over 600 m above sea level, typical of basement terrains marked by ridges and inselbergs (Ojo et al., 2024). Geologically, the area is dominated by migmatite–gneiss complexes, granitic intrusions, and minor schist belts, which are characteristic of the Nigerian Basement Complex and are widely associated with mineralization processes (Adetunla et al., 2025). These lithologies have undergone multiple episodes of deformation, metamorphism, and magmatism, resulting in well-developed structural features, including faults, fractures, and joints, which serve as conduits for hydrothermal fluids (Ogah & Abubakar, 2024). The occurrence of pegmatitic intrusions within the granitic units further enhances the area's mineralization potential, particularly for rare metals.

Climatically, the region falls within the tropical humid zone, with distinct wet and dry seasons and annual rainfall exceeding 1200 mm. Vegetation is mainly derived from a savannah with patches of secondary forest, which moderately affects surface exposure during geological and remote sensing investigations. The area is relatively accessible through a network of roads linking Ikole-Ekiti to other parts of Ekiti State. Overall, the favourable lithological composition, combined with a complex structural framework, makes the Ikole–Itapaji area a promising target for integrated geophysical and remote sensing studies to delineate zones of mineralization (Salako et al., 2024).

Field Description of the Study Area

Table 1 presents the field descriptions and geographic coordinates of seventeen (**17)** soil samples collected from different locations within the Ikole–Itapaji area of Southwestern Nigeria. The sampling points are spatially distributed across several settlements and farmland environments including Igbona-Ile, Agbeyewa Farm, Aba Farm, Esun, Omu, Iyemero, Odo-Oro, and Itapaji, thereby ensuring adequate representation of the study area. The geographic coordinates indicate that the sampled locations fall within latitudes 7°45′N to 7°59′N and longitudes 5°26′E to 5°33′E, reflecting a wide spatial coverage across the basement complex terrain. Elevation values vary considerably from 447 m to 588 m above sea level, suggesting moderate topographic variation within the study area, which may influence weathering intensity, drainage conditions, and elemental redistribution in the soils.

The sampled soils were collected at shallow depths ranging from 0.25 m to 0.60 m, representing near-surface regolith materials that are more susceptible to anthropogenic influence, weathering processes, and metal mobility. Field descriptions reveal considerable lithological and textural variability, with the soils comprising laterite, sandy clay, lateritic sand, gravelly sand, clayey sand, sandy loam, gravelly clay, and sand. Lateritic and reddish-brown soils dominate several locations such as SQ1, SQ6, SQ8, and SQ15, indicating intense tropical

ISSN No. 2454-6194 | DOI: 10.51584/IJRIAS |Volume XI Issue VI June 2026

weathering and iron oxide enrichment typical of Precambrian Basement Complex terrains. Brown to dark brown soil colours observed in many locations suggest varying proportions of organic matter, clay minerals, and iron-bearing constituents. The occurrence of gravelly and sandy materials in some sampling points further indicates active mechanical weathering and sediment reworking processes. Overall, the field characteristics demonstrate significant heterogeneity in soil composition and morphology across the study area, which is important for understanding heavy metal distribution, geochemical partitioning, and environmental behaviour within the different sequential extraction phases.

Table 1. Field Description and Geographic Coordinates of Soil Samples Collected from the Ikole–Itapaji Area, Southwestern Nigeria

S/N	Sample I	Locality	Latitude	Longitude	Elevation (m	Depth (m	Description	Colour
1	SQ1	Igbona-Ile, Ikol 1	7°45'41.9"	05°28'49.8"	564	0.35	Laterite	Reddish brown
2	SQ2	Igbona-Ile, Ikol 2	7°45'33.8"	05°26'53.6"	558	0.30	Sandy clay	Brown
3	SQ3	Ikole 1	7°46'23.3"	05°27'48.0"	550	0.50	Reddish brown soil	Reddish brown
4	SQ4	Agbeyewa farm	7°45'14.9"	05°28'12.6"	52	0.36	Sandy clay	Brown
5	SQ5	Ikole 2	7°50'55.8"	05°26'52.6"	556	0.40	Lateritic sand	Brown
6	SQ6	Aba farm	7°50'04.8"	05°28'16.1"	588	0.60	Laterite	Reddish brown
7	SQ7	Ikole 3	7°59'57.6"	05°27'24.0"	533	0.50	Sand	Brown
8	SQ8	Aba Dam	7°55'36.1"	05°27'42.0"	491	0.25	Laterite	Reddish brown
9	SQ9	Esun	7°45'14.9"	05°28'12.6"	541	0.28	Sandy clay	Brown
10	SQ10	Agbeyewa Farm	7°56'21.0"	05°30'20.0"	453	0.50	Gravelly sand	Grayish brown
11	SQ11	Aba Farm, Itapaji	7°58'47.0"	05°33'34.4"	447	0.34	Gravelly sand	Brown
12	SQ12	Aba Farm	7°54'23.1"	05°28'00.9"	481	0.40	Clayey sand	Brown
13	SQ13	Omu	7°53'18.9"	05°27'42.3"	503	0.30	Sand	Brown
14	SQ14	Itapaji	7°52'49.9"	05°31'05.2"	501	0.35	Sandy loam	Dark brown
15	SQ15	Iyemero	7°45'52.6"	05°33'06.3"	586	0.30	Laterite	Reddish brown

16	SQ16	Odo- Oro	7°49'45.0"	05°31'39.9"	578	0.35	Gravelly clay	Brown
17	SQ17	Ikole 4	7°50'46.3"	05°33'20.5"	543	0.40	Gravelly sand	Brown

Regional Geological Setting

The study area is located within southwestern Nigeria, forming part of the Precambrian Basement Complex of the West African Craton. This crystalline basement terrain is distinct from the surrounding sedimentary basins, including the Sokoto Basin, Chad Basin, Bida Basin, and the Benue Trough, which are largely composed of Cretaceous to Tertiary sediments (Ojo et al., 2024). The southwestern region, including the Ikole–Itapaji axis, is dominated by crystalline rocks that have undergone extensive tectono-metamorphic evolution. The Nigerian Basement Complex evolved through multiple orogenic events, notably the Liberian, Eburnean, and Pan-African cycles, which resulted in widespread deformation, metamorphism, and granitoid emplacement (Adetunla et al., 2025). These processes led to the development of major lithological units, including the migmatite–gneiss complex, schist belts, and Pan-African granitoids. In the study area, migmatite–gneiss and granitic rocks are predominant, with minor metasedimentary occurrences.

Structurally, the area is characterized by well-developed faults, fractures, and foliations, predominantly trending NE–SW and NW–SE, reflecting the imprint of the Pan-African deformational event (Ogah & Abubakar, 2024). These structures are critical in controlling hydrothermal fluid flow and mineral deposition. Mineralization within the Basement Complex is commonly associated with quartz veins, pegmatites, and shear zones. The presence of granitic and pegmatitic intrusions within the Ikole–Itapaji area further suggests favourable conditions for mineralization. Recent studies have demonstrated the effectiveness of integrated geophysical methods in delineating such structurally controlled mineralized zones (Salako et al., 2024). The geological framework of the study area reflects a complex interplay of lithology and structure, providing a suitable environment for mineralization and justification for integrated geophysical and remote sensing investigations **(Fig. 1)**

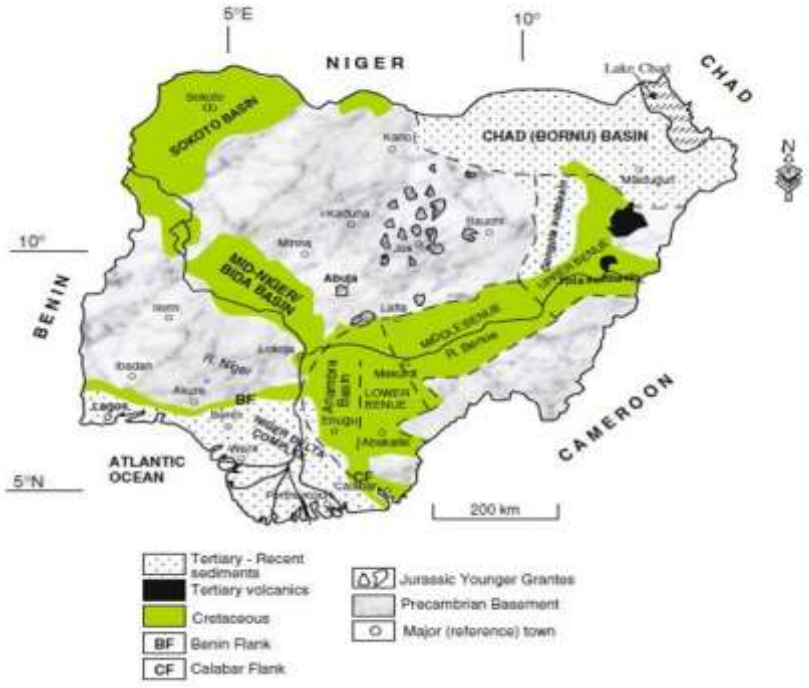

Figure 1: Geological map of Nigeria showing the distribution of major lithological units, including the Precambrian Basement Complex and surrounding sedimentary basins (Sokoto, Chad, Bida, and Benue Trough). The study area (Ikole–Itapaji, southwestern Nigeria) is located within the Basement Complex.

ISSN No. 2454-6194 | DOI: 10.51584/IJRIAS |Volume XI Issue VI June 2026

Geologic Map of the Study Area

The geological map of the study area reveals the major lithological units within the Precambrian Basement Complex of Southwestern Nigeria, particularly within the Ekiti basement terrain. The area has experienced complex tectonic, metamorphic, and magmatic activities associated mainly with the Pan-African orogeny (~600 ± 150 Ma) (Rahaman, 1988; Oyinloye, 2011). The dominant rock units include migmatite, granite gneiss, charnockite, and granodiorite.

Migmatite (Mg) occurs mainly in the southern and central portions around Ikole and Odo Oro. These rocks represent some of the oldest basement units and were formed through partial melting under high-grade metamorphic conditions. Granite gneiss (GG) is the most extensive lithology, occupying the northern, central, and western parts of the area, including Itapaji and Bolorunduro. These foliated granitic rocks are structurally competent and commonly host deformation features such as fractures and faults (Oyinloye, 2011).

Charnockite (Ch) occurs locally along the western margin of the study area and represents high-temperature granulite-facies rocks associated with deep crustal processes (Rahaman, 1988). Granodiorite (OGd) forms a major intrusive body within the north-central part of the area and belongs to the Older Granite suite emplaced during the late stages of the Pan-African orogeny. These intrusions commonly occupy structurally weak zones within the basement complex (Oyinloye, 2011) (**Fig. 2**).

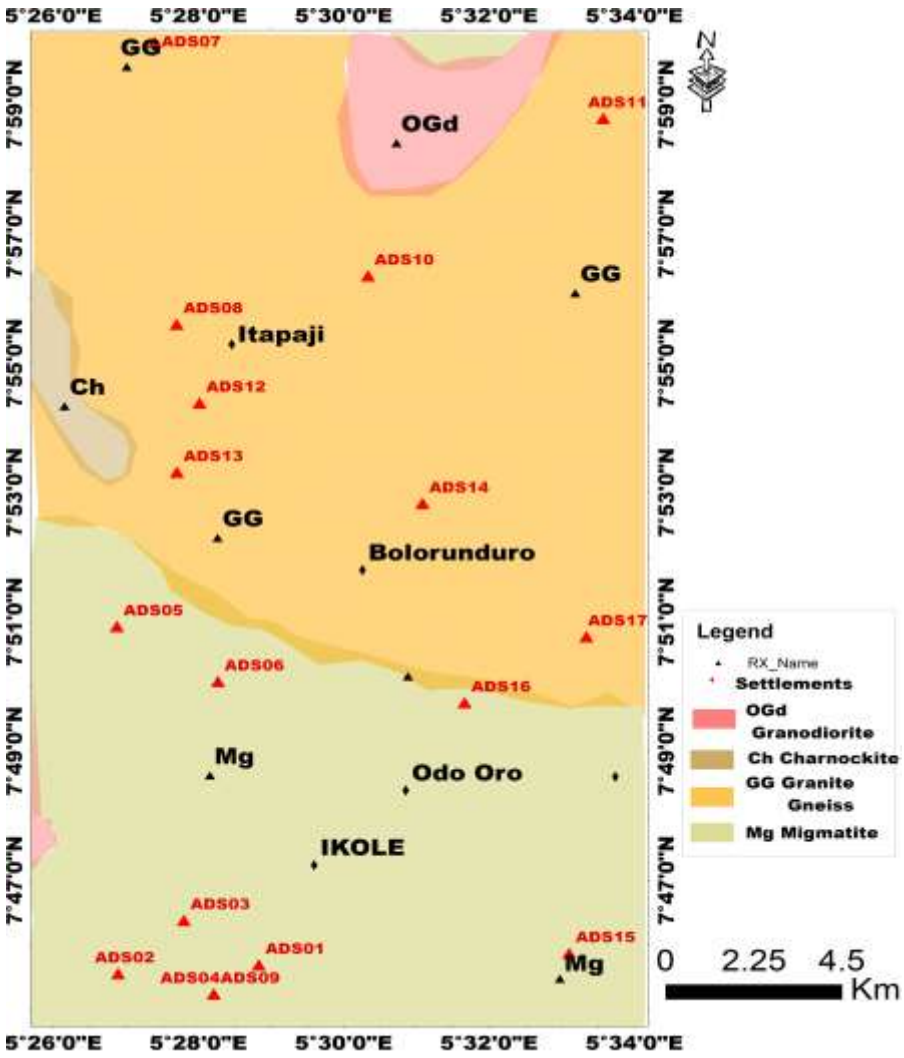

Figure 2: Geological map of the study area after NGSA (2006). The map delineates the distribution of major lithological units and their spatial relationships. It provides a foundational framework for structural interpretation and mineral exploration within the study area.

ISSN No. 2454-6194 | DOI: 10.51584/IJRIAS |Volume XI Issue VI June 2026

Sampling Points From the Study Area

The geological map illustrates the distribution of lithological units and soil sampling locations within the Ikole–Itapaji area of Southwestern Nigeria, covering approximately 16 km in the north–south direction and about 8 km east–west. The study area forms part of the Precambrian Basement Complex of Nigeria, which has undergone extensive tectonic, metamorphic, and magmatic activities associated with the Pan-African orogeny (Rahaman, 1988; Oyinloye, 2011). The mapped area encompasses major settlements including Ikole, Itapaji, Odo-Oro, and adjoining rural environments where detailed soil sampling was conducted.

The geological framework of the area is dominated by four major lithological units: granite gneiss (GG), migmatite (Mg), charnockite (Ch), and granodiorite (OGd). Granite gneiss constitutes the most extensive rock unit, occupying large portions of the northern, central, and western parts of the study area. Migmatite occurs mainly within the southern and southwestern sectors around Ikole and Odo-Oro, while charnockite is restricted to localized western portions of the map. Granodiorite occurs as a relatively small intrusive body within the north-central section of the study area. These lithological units represent important components of the Nigerian Basement Complex and significantly influence soil development, mineral composition, weathering intensity, and elemental distribution within the overlying regolith (Rahaman, 1988).

The soil sampling points (SQ1–SQ17) were strategically distributed across the various lithological terrains to ensure adequate spatial representation of the different parent rock materials. Some sampling locations such as SQ1, SQ3, and SQ15 are situated within migmatitic terrains, whereas SQ10 and SQ11 occur predominantly within granite gneiss zones. The sampling strategy also considered hydrological characteristics, as several points are located close to drainage channels and river networks in order to evaluate the possible influence of fluvial transport, leaching, and sediment redistribution on soil geochemistry. The integration of geological mapping with systematic soil sampling provides a valuable framework for understanding the relationship between bedrock lithology, weathering processes, soil development, and heavy metal distribution within the study area (**Fig. 3).**

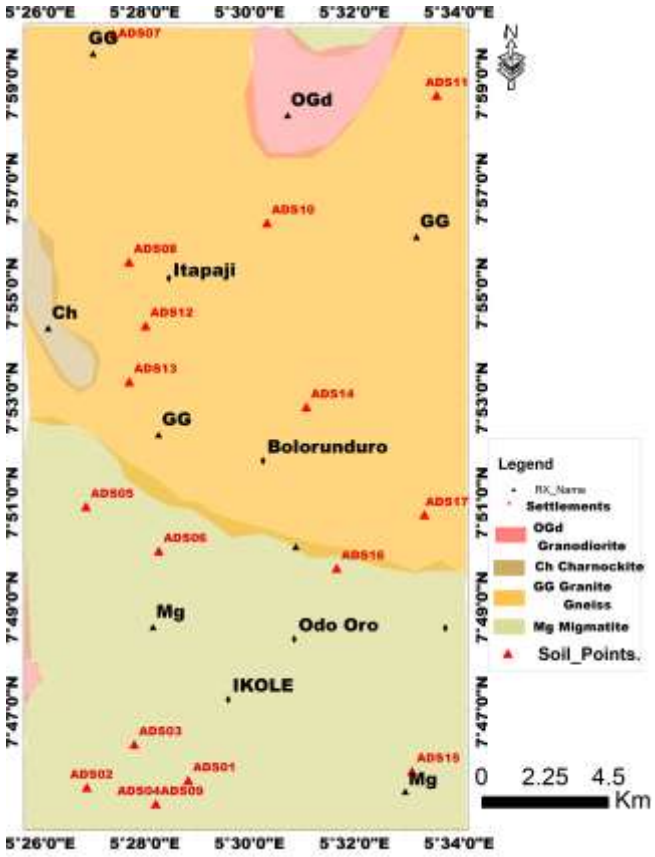

Figure 3. Geological map of the study area showing the distribution of lithological units and the locations of sampled points used for geological, geochemical, and petrographic investigations.

ISSN No. 2454-6194 | DOI: 10.51584/IJRIAS |Volume XI Issue VI June 2026

Materials And Methods

3.1 Sample Collection and Preparation

Soil/sediment samples were collected from selected locations within Ikole-Itapaji. The samples were obtained at shallow depths to represent the surficial geochemical environment of the study area. Each sample was air-dried at room temperature, gently disaggregated, and sieved to obtain the <63 µm fraction, which is known to retain higher concentrations of trace metals due to its large surface area and adsorption capacity.

A representative mass of 1.0 g of each prepared sample was weighed into clean centrifuge tubes for sequential extraction analysis.

3.2 Sequential Extraction Procedure

A seven-step sequential extraction procedure, modified from the widely adopted Tessier extraction scheme, was employed to partition metals into operationally defined geochemical fractions. This approach enables the differentiation of metals based on their binding strength and geochemical associations within sediments and soils. The procedure was designed to extract metals associated with water-soluble, exchangeable, carbonate-bound, Fe–Mn oxide-bound, organic-bound, sulfide/strongly bound, and residual phases.

Sequential extraction techniques have been widely applied in recent studies to evaluate the mobility, bioavailability, and environmental risk of trace metals in soils and sediments, as they provide more reliable information than total metal concentrations alone (De Matteis et al., 2023; Bouazizi et al., 2023). The method operates on the principle of selective dissolution, where specific reagents target distinct mineralogical or geochemical phases, allowing for detailed characterization of metal partitioning (Doi et al., 2023;). Recent modifications of the classical Tessier procedure have demonstrated improved efficiency, reproducibility, and applicability across diverse environmental matrices, including contaminated sediments and mining-impacted soils (Çelebi, 2024; Souza et al., 2024).

The adopted seven-step scheme provides enhanced resolution of metal speciation, particularly in distinguishing weakly bound fractions from those strongly incorporated within mineral lattices, thereby offering critical insights into both environmental behavior and mineralization processes.

The extraction steps were carried out as follows:

Phase 1: Water-Soluble Fraction
Twenty milliliters (20 mL) of deionized water was added to 1.0 g of sample and agitated for 1 hour at room temperature. The mixture was centrifuged, and the supernatant was decanted for analysis.

Phase 2: Exchangeable Fraction
Twenty milliliters (20 mL) of 1 M $MgCl_2$ solution was added to the residue from Phase 1 and shaken for 1 hour. The mixture was centrifuged, and the extract was collected.

Phase 3: Carbonate-Bound Fraction
Twenty milliliters (20 mL) of 1 M sodium acetate (NaOAc) adjusted to pH 5 was added to the residue from Phase 2 and shaken for 5 hours. After centrifugation, the extract was filtered and preserved.

Phase 4: Fe–Mn Oxide (Reducible) Fraction
Twenty milliliters (20 mL) of hydroxylamine hydrochloride ($NH_2OH \cdot HCl$) solution was added to the residue from Phase 3 and heated at approximately 95°C for 2 hours with intermittent agitation. The mixture was cooled, centrifuged, and the extract was collected.

Phase 5: Organic Matter-Bound Fraction
Ten milliliters (10 mL) of acidified hydrogen peroxide (H_2O_2) was added to the residue from Phase 4 and

ISSN No. 2454-6194 | DOI: 10.51584/IJRIAS |Volume XI Issue VI June 2026

heated at 85°C for 2 hours. A second aliquot of 10 mL H_2O_2 was added, followed by repeated heating. After cooling, 20 mL of ammonium acetate (NH_4OAc) was added, and the mixture was shaken for 30 minutes before centrifugation and collection of the extract.

Phase 6: Sulfide/Strongly Bound Fraction
Fifteen milliliters (15 mL) of concentrated nitric acid (HNO_3) was added to the residue from Phase 5 and heated gently to near dryness. The residue was cooled, diluted, centrifuged, and the extract was collected.

Phase 7: Residual Fraction
The final residue was digested using a mixture of hydrofluoric acid (HF), perchloric acid ($HClO_4$), and nitric acid (HNO_3) until complete dissolution was achieved. The digest was appropriately diluted for analysis.

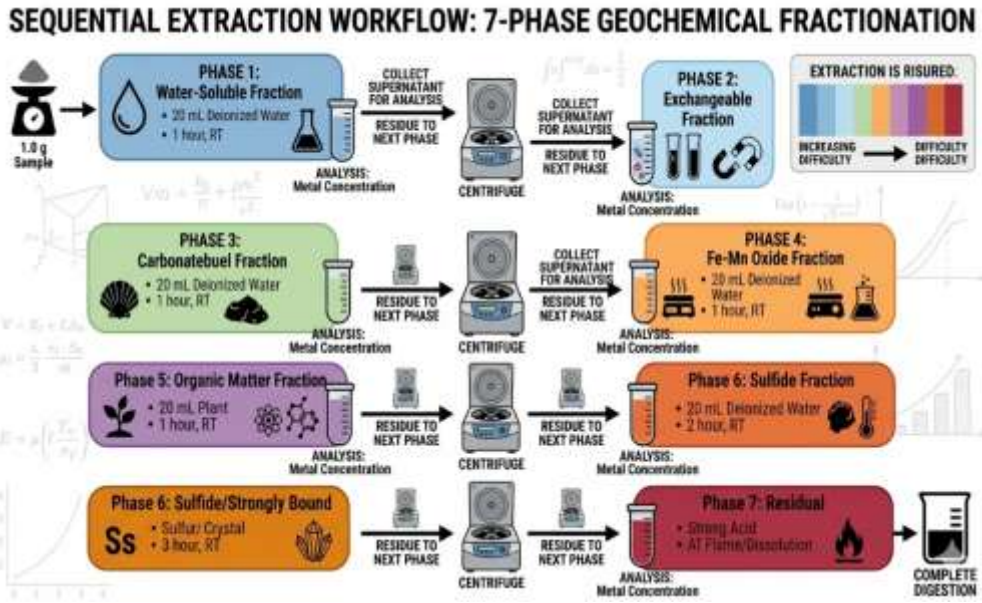

3.3 Geochemical Pollution Indices

Trace metal concentrations were determined using Atomic Absorption Spectrophotometry **(AAS)** (Buck Scientific Model 205A) with an air–acetylene flame. Calibration standards were prepared using appropriate matrix-matched solutions to ensure analytical accuracy.

For each fraction, the supernatant was diluted where necessary (typically 20–50×), and concentrations were obtained from calibration curves. All analyses were conducted in triplicate, and reagent blanks were included to ensure quality control.

For total metal determination (residual fraction), samples were subjected to strong acid digestion using HF–$HClO_4$–HNO_3 mixtures to ensure complete dissolution of silicate matrices, following standard geochemical digestion protocols.

Contamination Factor (CF)

- The Contamination Factor (CF) was used to assess the level of metal contamination relative to natural background (shale) concentrations **Table 2.** It was calculated using the relationship:
- $CF = Csample / Cbackground$ (1)

where:
Csample represents the measured concentration of a metal in the sample, Background represents the corresponding background concentration (average shale value) (**Table 2).**

ISSN No. 2454-6194 | DOI: 10.51584/IJRIAS |Volume XI Issue VI June 2026

- CF values indicate the degree of contamination of individual metals, where values greater than 1 suggest anthropogenic influence, while values less than 1 indicate natural background levels.

Pollution Load Index (PLI)

- The Pollution Load Index (PLI) was used to evaluate the overall level of heavy metal pollution at each sampling location. It was calculated using the relationship:
- $PLI = (CF1 \times CF2 \times CF3 \times \ldots \times CFn)^{(1/n)}$ (2)
- where:
  CF1–CFn represent the contamination factors of individual metals, n represents the number of metals analyzed.
- PLI provides a cumulative indication of the overall pollution status of a site, where values equal to 1 indicate baseline conditions, values less than 1 indicate no pollution, and values greater than 1 indicate deterioration of environmental quality.

Table 2. Average shale values of selected heavy metals used as geochemical background concentrations for pollution assessment in the study area (Turekian and Wedepohl, 1961).

S/N	Metal	Shale Value (mg/kg)
1	Fe	47,200
2	Mn	850
3	Pb	20
4	Cu	45
5	Zn	95
6	Ni	68
7	Co	19
8	Cr	90
9	Cd	0.3

RESULTS AND DISCUSSION

Water-Soluble Phase

The water-soluble phase represents the most mobile and bioavailable fraction of metals in soils and sediments, and it is typically very low in natural systems due to strong mineral binding (Kabata-Pendias, 2011; Alloway, 2013).

Results in **Table 3a** show generally low concentrations of all metals across samples (SQ1–SQ17), indicating limited dissolution into pore water. Fe records the highest values (2.873–7.427 mg/kg), reflecting relatively higher geochemical reactivity but still low mobility due to strong association with silicate and oxide minerals.

ISSN No. 2454-6194 | DOI: 10.51584/IJRIAS |Volume XI Issue VI June 2026

Mn ranges from 1.742–3.128 mg/kg, showing slight variation linked to redox sensitivity (Reimann & de Caritat, 2012). Cu (0.163–0.742 mg/kg) and Zn (0.126–0.627 mg/kg) are low, suggesting natural weathering control, while Pb (0.049–0.098 mg/kg) and Cd (0.002–0.007 mg/kg) indicate minimal contamination and strong retention in solid phases. Ni, Co, and Cr also remain consistently low across samples.

The statistical summary in **Table 3b** confirms low variability, with mean concentrations ordered as Fe > Mn > Cu ≈ Zn > Pb > Co ≈ Ni > Cr > Cd. This indicates dominance of lithogenic control with very limited metal mobility. The spatial distribution shown in **Figure 4** (cluster column chart**)** supports these observations, clearly illustrating the dominance of Fe and Mn across all samples. At the same time, other metals remain uniformly low with no distinct spatial anomaly. The clustering pattern confirms that variations are minor and do not reflect pollution hotspots but natural geochemical background levels.

Overall, the combined interpretation of **Table 3a, Table 3b, and Figure 4** indicates low mobility, weak aqueous dispersion, and strong lithogenic control of metals in the water-soluble phase, with negligible environmental risk under current conditions.

Table 3a. Heavy metals concentration in the water-soluble phase (mg/kg) of sediments/soils from the Ikole–Itapaji area, Southwestern Nigeria. This fraction represents the most mobile and immediately bioavailable portion of trace metals, reflecting their potential short-term environmental availability and mobility in the near-surface environment.

Samples	Fe	Mn	Pb	Cu	Zn	Ni	Co	Cr	Cd
	(mg/Kg)	(mg/Kg)	(mg/Kg)	(mg/Kg)	**(**mg/Kg)	(mg/Kg)	(mg/Kg)	(mg/Kg)	(mg/Kg)
SQ 1	6.321	2.087	0.077	0.681	0.572	0.054	0.062	0.023	0.004
SQ 2	6.128	2.063	0.072	0.631	0.509	0.059	0.063	0.021	0.003
SQ 3	7.427	3.108	0.083	0.724	0.592	0.063	0.069	0.028	0.005
SQ 4	7.129	3.099	0.081	0.711	0.579	0.061	0.066	0.025	0.005
SQ 6	5.873	2.145	0.094	0.742	0.582	0.063	0.067	0.029	0.006
SQ7	4.568	1.958	0.064	0.465	0.368	0.043	0.048	0.016	0.003
SQ 8	6.409	2.056	0.076	0.641	0.539	0.052	0.063	0.022	0.004
SQ 10	2.873	1.742	0.049	0.163	0.126	0.034	0.037	0.013	0.002
SQ 11	3.208	1.839	0.056	0.218	0.189	0.041	0.045	0.015	0.003
SQ 12	5.175	2.094	0.086	0.598	0.565	0.061	0.057	0.024	0.005
SQ 13	5.387	2.109	0.087	0.605	0.591	0.063	0.054	0.026	0.005
SQ 14	6.125	2.135	0.092	0.676	0.608	0.067	0.061	0.029	0.006
SQ 15	7.105	3.128	0.091	0.624	0.573	0.056	0.054	0.031	0.006
SQ 16	5.891	2.207	0.095	0.673	0.606	0.065	0.059	0.034	0.007
SQ 17	5.006	1.876	0.098	0.659	0.627	0.064	0.062	0.033	0.007

ISSN No. 2454-6194 | DOI: 10.51584/IJRIAS |Volume XI Issue VI June 2026

Table 3b. Statistical summary of the heavy metals concentration in the water-soluble phase (mg/kg). This table presents the minimum, maximum, and mean concentrations of the selected metals across all samples in the study area. It provides a simplified statistical overview of metal distribution and mobility within the most labile geochemical fraction of the soil–sediment system.

Metal	Fe	Mn	Pb	Cu	Zn	Ni	Co	Cr	Cd
Min	2.873	1.742	0.049	0.163	0.126	0.034	0.037	0.013	0.002
Max	7.427	3.128	0.098	0.742	0.627	0.067	0.069	0.034	0.007
Mean	5.642	2.243	0.080	0.587	0.508	0.056	0.058	0.025	0.005

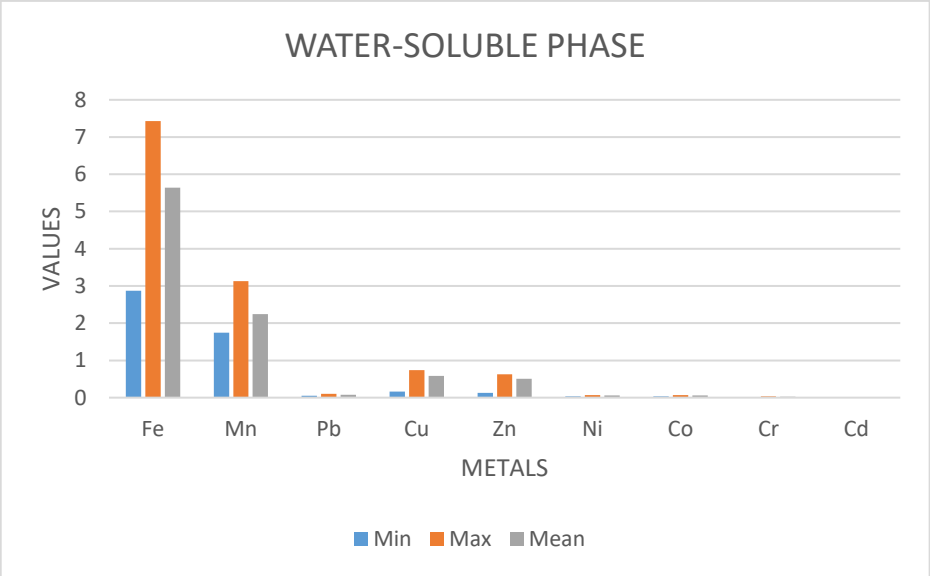

Figure 4. Cluster column chart of heavy metal concentrations in the water-soluble phase (mg/kg). The figure illustrates the comparative distribution of selected metals across all samples, highlighting variations in their mobility and relative abundance within the most labile geochemical fraction.

The exchangeable phase

The exchangeable phase consists of metals weakly adsorbed to soil surfaces and is environmentally important because such metals can be released under changes in pH, ionic strength, or competing ions (Kabata-Pendias, 2011; Alloway, 2013).

Table 4a shows higher metal concentrations than the water-soluble phase, indicating stronger but reversible adsorption to soil exchange sites. Fe is dominant (5.731–10.742 mg/kg), reflecting strong association with clay and oxide minerals. Mn (1.342–3.127 mg/kg) shows moderate variability linked to redox sensitivity (Alloway, 2013).

Cu (0.279–0.967 mg/kg) and Zn (0.261–0.886 mg/kg) are moderately retained, while Pb (0.082–0.146 mg/kg) and Cd (0.004–0.029 mg/kg) remain low but slightly enriched, indicating potential mobility under acidic conditions. Ni, Co, and Cr are consistently low, reflecting partial release from primary minerals. **Table 4b** shows the mean order:
Fe > Mn > Cu > Zn > Pb > Ni > Co > Cr > Cd, confirming Fe and Mn dominance.

ISSN No. 2454-6194 | DOI: 10.51584/IJRIAS |Volume XI Issue VI June 2026

Spatially, SQ3, SQ4, SQ14, SQ15, and SQ17 show higher values, while SQ10 is the lowest, suggesting natural lithological control rather than contamination. This pattern is supported by **Figure 5**, which highlights clear Fe–Mn dominance, moderate Cu–Zn clustering, and uniformly low Pb, Cd, Ni, Co, and Cr across samples.

Overall, the exchangeable phase exhibits moderate metal retention and limited mobility, controlled primarily by clay minerals and organic matter. The presence of Pb and Cd, though low, indicates potential sensitivity to environmental changes such as acidification (Kabata-Pendias, 2011; Alloway, 2013).

Table 4a: Exchangeable phase of the heavy metal concentrations in soil samples (mg/kg). The table presents the distribution of Fe, Mn, Pb, Cu, Zn, Ni, Co, Cr, and Cd across all sampling locations, reflecting metals weakly bound to soil exchange sites and their potential environmental mobility.

Samples	Fe	Mn	Pb	Cu	Zn	Ni	Co	Cr	Cd
	(mg/Kg)	(mg/Kg)	(mg/Kg)	(mg/Kg)	**(mg/Kg)**	(mg/Kg)	(mg/Kg)	(mg/Kg)	(mg/Kg)
SQ 1	8.084	1.875	0.098	0.789	0.701	0.072	0.071	0.031	0.007
SQ 2	8.005	1.802	0.097	0.712	0.685	0.073	0.069	0.032	0.005
SQ 3	10.742	2.085	0.102	0.826	0.732	0.081	0.075	0.037	0.029
SQ 4	10.488	2.016	0.108	0.813	0.735	0.085	0.076	0.037	0.028
SQ 6	6.402	2.073	0.112	0.839	0.784	0.082	0.073	0.042	0.009
SQ7	6.023	1.762	0.082	0.619	0.586	0.065	0.059	0.025	0.005
SQ 8	8.787	1.904	0.126	0.804	0.721	0.075	0.073	0.034	0.026
SQ 10	5.731	1.342	0.085	0.279	0.261	0.067	0.072	0.026	0.004
SQ 11	6.174	1.563	0.096	0.351	0.31	0.071	0.072	0.029	0.005
SQ 12	7.787	2.012	0.113	0.801	0.721	0.094	0.087	0.038	0.009
SQ 13	7.819	2.105	0.109	0.799	0.726	0.097	0.085	0.042	0.01
SQ 14	8.534	3.083	0.138	0.902	0.846	0.102	0.095	0.051	0.017
SQ 15	10.231	3.127	0.146	0.927	0.872	0.117	0.102	0.054	0.021
SQ 16	7.118	2.105	0.128	0.942	0.839	0.112	0.11	0.059	0.028
SQ 17	6.104	2.098	0.131	0.967	0.886	0.132	0.121	0.061	0.026

Table 4b: Statistical summary of the heavy metals concentration in the exchangeable phase (mg/kg). This table presents the minimum, maximum, and mean concentrations of selected metals across all samples in the exchangeable fraction. It highlights the variability and relative mobility of metals weakly bound to soil exchange sites, which are potentially available for environmental release.

Metal	**Fe**	**Mn**	**Pb**	**Cu**	**Zn**	**Ni**	**Co**	**Cr**	**Cd**
Min	5.731	1.342	0.082	0.279	0.261	0.065	0.059	0.025	0.004

Metal	Fe	Mn	Pb	Cu	Zn	Ni	Co	Cr	Cd
Max	10.742	3.127	0.146	0.967	0.886	0.132	0.121	0.061	0.029
Mean	7.869	2.064	0.111	0.758	0.694	0.088	0.083	0.040	0.015

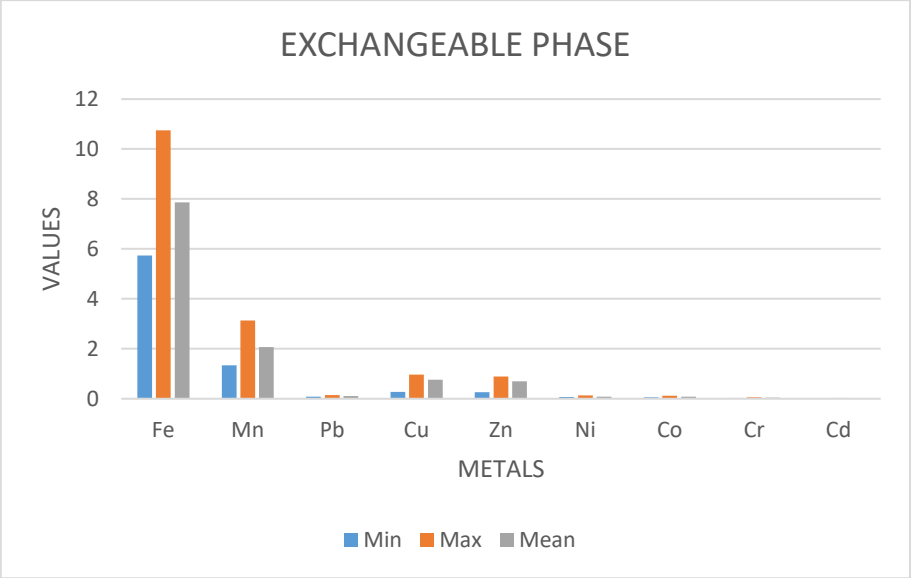

Figure 5. Cluster column chart of heavy metal concentrations in the exchangeable phase (mg/kg). The figure illustrates the comparative distribution of metals across all samples in the exchangeable fraction, highlighting variations in their relative mobility and binding strength to soil exchange sites.

The carbonate-bound phase

The carbonate-bound phase comprises metals associated with carbonate minerals and is sensitive to pH changes, particularly under acidic conditions where dissolution can release bound metals (Kabata-Pendias, 2011; Alloway, 2013).

Table 5a shows a clear increase in metal concentrations compared to earlier fractions, indicating stronger incorporation into carbonate phases. Fe (36.325–66.488 mg/kg) and Mn (23.728–38.019 mg/kg) dominate, reflecting their affinity for co-precipitation with carbonates. Zn (12.101–19.807 mg/kg) and Cu (1.112–3.213 mg/kg) show moderate enrichment, while Pb (1.025–3.832 mg/kg) indicates stable carbonate association. Ni, Co, and Cr occur at lower but consistent levels, and Cd remains low (0.054–0.121 mg/kg). The statistical summary in **Table 5b** confirms the trend: Fe > Mn > Zn > Pb > Cu > Ni > Co > Cr > Cd

Spatially, higher values in SQ3, SQ4, and SQ15 contrast with lower concentrations in SQ10, reflecting lithological variability rather than contamination. This pattern is supported by **Figure 6**, which highlights Fe–Mn dominance, moderate Zn–Cu enrichment, and consistently lower levels of other metals across samples. Overall, the carbonate-bound phase represents a moderately stable metal reservoir with potential mobility under acidic conditions, although current distributions indicate strong lithogenic control.

Table 5a. Heavy metal concentrations in the carbonate-bound phase (mg/kg). The table shows the distribution of metals associated with carbonate minerals across all samples, reflecting their relative stability and potential release under acidic environmental conditions.

Samples	Fe	Mn	Pb	Cu	Zn	Ni	Co	Cr	Cd

ISSN No. 2454-6194 | DOI: 10.51584/IJRIAS |Volume XI Issue VI June 2026

	(mg/Kg)	(mg/Kg)	(mg/Kg)	(mg/Kg)	(mg/Kg)	(mg/Kg)	(mg/Kg)	(mg/Kg)	(mg/Kg)
SQ 1	40.129	25.207	2.279	2.439	13.226	2.147	1.701	0.531	0.069
SQ 2	41.052	25.422	2.142	2.197	13.055	2.132	1.626	0.625	0.065
SQ 3	65.246	37.529	3.217	2.826	18.614	2.704	2.002	0.954	0.089
SQ 4	66.488	38.019	3.832	3.213	18.901	3.125	2.106	1.005	0.103
SQ 6	38.615	24.234	1.715	2.327	13.178	2.362	1.448	0.603	0.059
SQ7	38.247	24.127	1.665	2.401	13.218	2.295	1.353	0.616	0.055
SQ 8	41.271	25.431	3.102	2.424	13.286	2.149	1.747	1.103	0.072
SQ 10	36.325	23.728	1.025	1.112	12.521	1.891	0.829	0.518	0.054
SQ 11	37.623	24.061	2.611	2.103	12.101	2.047	1.521	0.556	0.055
SQ 12	39.114	25.716	3.112	2.518	12.224	2.104	1.687	0.738	0.069
SQ 13	38.864	24.612	3.109	2.429	12.138	2.049	1.716	0.742	0.071
SQ 14	41.451	26.128	2.234	2.657	13.441	2.162	1.392	0.671	0.077
SQ 15	46.539	37.423	3.627	2.985	19.807	3.127	2.108	1.054	0.121
SQ 16	41.318	25.035	2.512	2.548	13.033	2.102	1.711	1.005	0.098
SQ 17	38.712	24.291	2.271	2.462	12.987	1.937	1.491	0.657	0.097

Table 5b. Statistical summary of the heavy metals in the carbonate-bound phase (mg/kg). The table presents the minimum, maximum, and mean concentrations of metals associated with carbonate fractions, highlighting their relative enrichment and stability within this geochemical phase.

Metal	**Fe**	**Mn**	**Pb**	**Cu**	**Zn**	**Ni**	**Co**	**Cr**	**Cd**
Min	36.325	23.728	1.025	1.112	12.101	1.891	0.829	0.518	0.054
Max	66.488	38.019	3.832	3.213	19.807	3.127	2.108	1.103	0.121
Mean	43.580	26.998	2.630	2.450	13.915	2.235	1.629	0.758	0.078

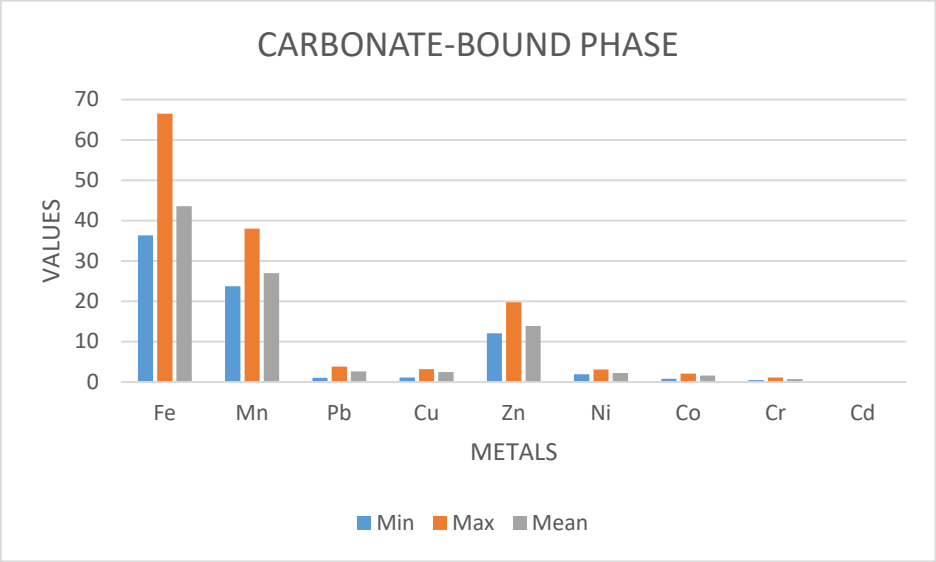

Figure 6. Cluster column chart of the heavy metal concentrations in the carbonate-bound phase (mg/kg). **The** figure illustrates the comparative distribution of metals across all samples, highlighting their relative enrichment and association with carbonate minerals within this geochemical fraction.

The Fe–Mn oxide phase

Table 6a and 6b present the distribution and statistical summary of heavy metals associated with the Fe–Mn oxide fraction across the studied soil samples. This geochemical phase is particularly important because iron and manganese oxides are known to have strong adsorption capacities and therefore act as major sinks for trace metals in soil environments (Kabata-Pendias, 2011; Alloway, 2013). The results show that Fe and Mn occur in relatively high concentrations across all samples, with Fe ranging from 303.187 to 476.031 mg/kg and Mn from 139.204 to 267.163 mg/kg. These elevated values reflect the dominance of Fe–Mn oxides in controlling metal retention and indicate strong scavenging of trace elements during secondary soil-forming processes.

Among the trace metals, Zn shows comparatively higher concentrations (54.584–77.129 mg/kg), followed by Pb (16.623–36.125 mg/kg), Cu (11.197–22.957 mg/kg), and Ni (16.352–26.103 mg/kg). Co, Cr, and Cd occur at lower but still significant levels, indicating variable affinity for Fe–Mn oxide surfaces. The highest metal loadings are observed in samples SQ3, SQ4, and SQ15, suggesting localized enrichment possibly linked to lithological variation or enhanced adsorption under specific geochemical conditions. In contrast, samples such as SQ10 consistently record the lowest concentrations, indicating weaker metal retention capacity in those locations.

The statistical summary (Table 4b) further confirms the strong geochemical association of metals with Fe–Mn oxides, with mean concentrations following the order Fe > Mn > Zn > Pb > Cu > Ni > Co > Cr > Cd. The relatively high mean values of Zn, Pb, and Cu suggest significant anthropogenic influence superimposed on natural geochemical processes. Overall, the Fe–Mn oxide fraction plays a critical role in controlling metal mobility and redistribution in the study area, as these oxides can effectively adsorb and immobilize trace metals under varying redox conditions (Tessier et al., 1979; Wei & Yang, 2010).

Table 6a: Heavy metal concentrations in the Fe–Mn oxide phase (mg/kg**).** The table presents the distribution of metals associated with iron and manganese oxides across all samples, reflecting their strong adsorption capacity and role as key geochemical sinks for trace elements.

Samples	Fe	Mn	Pb	Cu	Zn	Ni	Co	Cr	Cd
	(mg/Kg)	(mg/Kg)	(mg/Kg)	(mg/Kg)	**(mg/Kg)**	(mg/Kg)	(mg/Kg)	(mg/Kg)	(mg/Kg)
SQ 1	354.813	152.227	25.711	13.403	63.866	19.181	10.271	6.361	0.621

SQ 2	361.558	175.129	22.019	15.019	63.545	20.196	11.287	6.185	0.657
SQ 3	435.209	237.214	33.277	20.236	74.091	22.573	14.263	9.159	1.872
SQ 4	446.513	241.116	35.332	21.873	77.129	26.103	14.742	10.015	1.983
SQ 6	362.145	154.434	26.072	12.615	63.071	20.032	10.481	5.235	0.598
SQ7	358.903	149.828	21.612	13.211	63.242	18.269	9.593	6.062	0.615
SQ 8	371.874	185.401	26.128	14.029	70.008	20.542	11.792	8.187	1.328
SQ 10	303.187	139.204	16.623	11.197	54.584	16.352	6.282	4.815	0.574
SQ 11	337.217	144.436	18.217	12.018	58.611	19.142	8.027	5.251	0.591
SQ 12	349.812	147.164	23.712	16.182	62.202	20.017	10.019	6.131	0.691
SQ 13	345.875	147.119	23.389	16.429	62.138	20.049	9.948	5.782	0.711
SQ 14	360.158	176.524	25.304	15.173	63.493	21.366	11.097	7.176	0.877
SQ 15	476.031	267.163	36.125	22.957	75.937	25.183	13.162	10.254	2.021
SQ 16	361.521	155.003	22.574	14.348	64.113	19.179	11.201	7.012	0.798
SQ 17	338.019	142.401	17.753	12.967	59.285	18.331	10.096	8.954	0.917

Table 6b: Statistical summary of the heavy metals concentration in the Fe–Mn oxide phase (mg/kg). The table shows the minimum, maximum, and mean concentrations of metals bound to Fe–Mn oxides, highlighting their significant enrichment and strong affinity for adsorption within this geochemical fraction.

Metal	**Fe**	**Mn**	**Pb**	**Cu**	**Zn**	**Ni**	**Co**	**Cr**	**Cd**
Min	303.187	139.204	16.623	11.197	54.584	16.352	6.282	4.815	0.574
Max	476.031	267.163	36.125	22.957	77.129	26.103	14.742	10.254	2.021
Mean	370.456	173.958	24.790	15.977	65.554	20.454	10.751	7.122	0.923

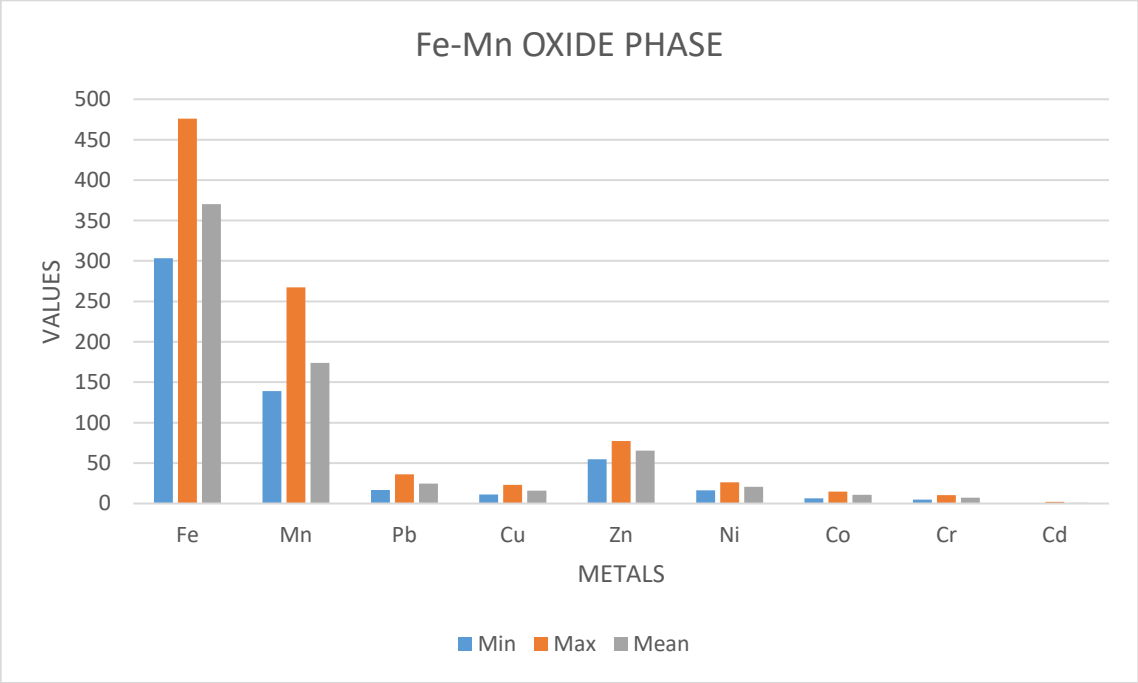

Figure 7. Cluster column chart of the heavy metal concentrations in the Fe–Mn oxide phase (mg/kg). The figure illustrates the comparative distribution of metals across all samples, highlighting strong enrichment and adsorption of trace elements onto Fe–Mn oxide phases within the study area.

ISSN No. 2454-6194 | DOI: 10.51584/IJRIAS |Volume XI Issue VI June 2026

The Organic Matter–Bound Phase

The organic matter–bound phase represents metals complexed with humic substances, decomposed organic residues, and microbial materials, and it acts as an important intermediate sink controlling metal retention and delayed release during organic matter decomposition. In tropical soils, this fraction is enhanced by high organic turnover and redox fluctuations, which promote metal–organic complex formation (Kaiser & Kalbitz, 2012; Liu et al., 2022).

From **Table 7a**, Fe shows the highest concentrations (148.854–356.163 mg/kg), indicating strong complexation with organic ligands. Mn (55.772–89.112 mg/kg) also shows appreciable association, reflecting its redox-sensitive behavior influenced by organic matter (Liu et al., 2022). Among trace metals, Cu (14.158–24.486 mg/kg) and Zn (24.128–40.372 mg/kg) are relatively enriched, confirming their strong affinity for organic functional groups. Pb (9.926–16.562 mg/kg) and Cd (0.414–1.221 mg/kg) occur at lower levels but remain environmentally important due to their potential remobilization during organic matter decomposition.

Ni, Co, and Cr show moderate association with organic matter, suggesting partial complexation and mixed control by both organic and mineral phases. The statistical summary in **Table 7b** confirms the dominance order: Fe > Mn > Zn > Cu > Ni ≈ Pb > Co > Cr > Cd, highlighting Fe and Mn as the major contributors to this fraction (Birth, (2003).

Spatially, higher concentrations in SQ3, SQ4, and SQ15 suggest zones with stronger organic matter influence, while lower values in SQ6 and SQ10 reflect weaker organic binding. **Figure 8** shows a similar pattern, with Fe and Mn dominating, followed by Cu and Zn, while Pb, Cd, Ni, Co, and Cr remain comparatively low.

Overall, this phase indicates that organic matter plays a key role in stabilizing metals—especially Cu, Zn, Fe, and Mn—while also serving as a potential secondary source under decomposition or changing redox conditions (Alloway, 2013; Kaiser & Kalbitz, 2012).

Table 7a: Heavy metals concentrations in the organic matter–bound phase (mg/kg). The table shows the distribution of metals associated with organic matter across all samples, reflecting their affinity for organic complexation and potential release during organic matter decomposition.

Samples	Fe	Mn	Pb	Cu	Zn	Ni	Co	Cr	Cd
	(mg/Kg)	(mg/Kg)	(mg/Kg)	(mg/Kg)	(mg/Kg)	(mg/Kg)	(mg/Kg)	(mg/Kg)	(mg/Kg)
SQ 1	182.012	75.224	12.172	20.032	33.213	12.817	6.915	5.503	0.453
SQ 2	181.654	78.127	13.181	20.215	33.158	13.102	6.429	6.232	0.485
SQ 3	335.147	87.225	14.137	22.864	37.685	16.214	8.105	6.954	0.981
SQ 4	341.401	89.112	16.562	23.509	40.021	18.121	9.012	7.051	1.128
SQ 6	164.319	64.435	10.345	15.861	27.183	10.129	4.971	4.672	0.429
SQ7	168.247	64.247	10.631	15.539	28.011	10.216	5.056	4.956	0.433
SQ 8	189.074	81.236	13.123	20.421	33.786	13.014	6.747	6.143	0.472
SQ 10	148.854	55.772	9.926	14.158	24.128	8.997	4.635	4.329	0.414
SQ 11	152.627	57.201	10.011	15.141	25.091	9.089	4.921	4.457	0.425

ISSN No. 2454-6194 | DOI: 10.51584/IJRIAS |Volume XI Issue VI June 2026

SQ 12	169.612	65.236	11.162	16.214	25.274	10.176	5.068	4.781	0.446
SQ 13	169.881	64.837	11.134	16.452	25.181	10.089	5.112	8.714	0.451
SQ 14	180.575	76.294	12.634	21.052	32.846	12.763	6.557	5.773	0.472
SQ 15	356.163	87.826	15.663	24.486	40.372	18.522	9.138	7.074	1.221
SQ 16	185.052	75.135	12.246	20.415	33.325	13.012	6.751	6.028	0.482
SQ 17	168.176	65.095	10.773	15.404	28.197	10.332	6.904	6.193	0.462

Table 7b: Statistical summary of the heavy metals in the organic matter–bound phase (mg/kg). The table presents the minimum, maximum, and mean concentrations of metals associated with organic matter, indicating their degree of complexation and relative stability within this geochemical fraction.

Metal	Fe	Mn	Pb	Cu	Zn	Ni	Co	Cr	Cd
Min	148.854	55.772	9.926	14.158	24.128	8.997	4.635	4.329	0.414
Max	356.163	89.112	16.562	24.486	40.372	18.522	9.138	8.714	1.221
Mean	206.186	72.467	12.247	18.784	31.165	12.440	6.421	5.924	0.584

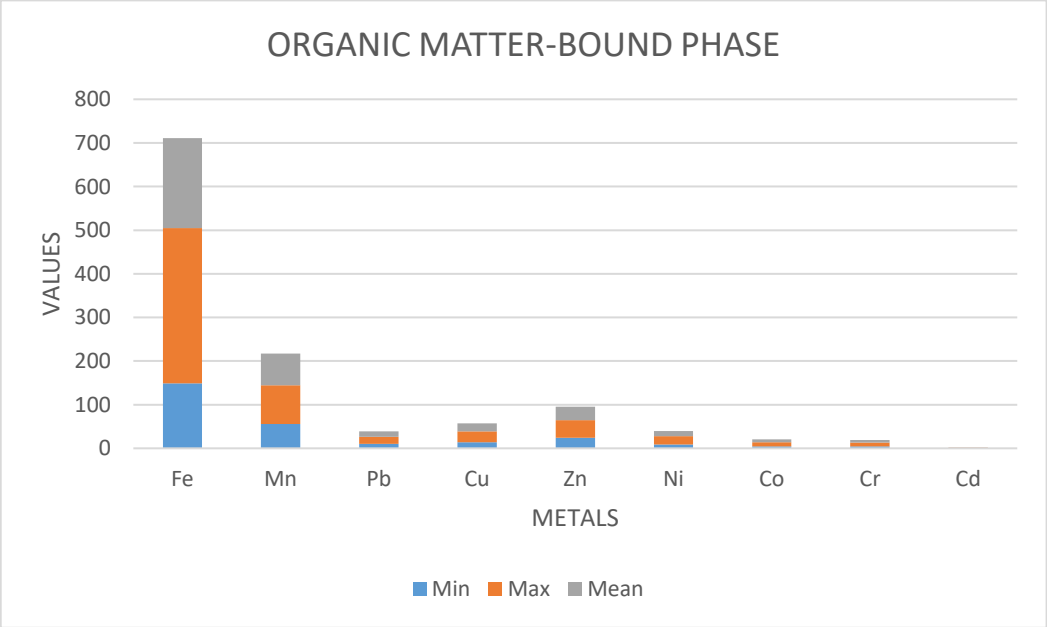

Figure 8. Cluster column chart of the heavy metal concentrations in the organic matter–bound phase (mg/kg). The figure illustrates the distribution of metals across all samples, highlighting their association with organic matter and relative enrichment through complexation with organic ligands.

The Sulfide/Strongly Bound Phase

The sulfide/strongly bound phase represents metals incorporated into sulfide minerals and resistant mineral lattices, and it is generally regarded as the most stable and least mobile fraction in sequential extraction studies. Metals in this fraction are only released under strong oxidizing conditions, making it a long-term geochemical sink for trace elements in soils and sediments (Tessier et al., 1979;).

ISSN No. 2454-6194 | DOI: 10.51584/IJRIAS |Volume XI Issue VI June 2026

From **Table 8a**, Fe shows the highest concentrations (184.382–353.506 mg/kg), indicating strong incorporation into resistant and sulfide-related mineral phases. Mn (75.148–150.084 mg/kg) also shows significant association, reflecting co-precipitation under reducing conditions. Among trace metals, Zn (22.101–37.022 mg/kg) and Cu (12.503–22.129 mg/kg) show moderate enrichment, consistent with their known affinity for sulfide mineral formation. Pb (11.016–25.791 mg/kg) is also appreciable, while Cd remains low (0.312–1.147 mg/kg), reflecting its weaker sulfide stability (Birth, (2003).

Ni, Co, and Cr occur at moderate levels, suggesting partial incorporation into resistant mineral phases. The statistical summary **Table 8b** confirms the dominance order: Fe > Mn > Zn > Cu > Pb > Ni > Co > Cr > Cd, indicating strong geochemical stabilization of Fe and Mn in this fraction (Hakanson, (1980).

Spatially, higher values in SQ3, SQ4, and SQ15 suggest localized reducing conditions or sulfide enrichment, while lower values in SQ6 and SQ10 indicate weaker sulfide association. **Figure 9** shows the same pattern, with Fe and Mn dominating across all samples. Overall, this phase represents a stable metal reservoir with low immediate mobility, though it may become a secondary source of metals under oxidative environmental changes (Davidson et al., 1994;).

Table 8a: Heavy metal concentrations in the sulfide/strongly bound phase (mg/kg). The table shows metals strongly associated with sulfide minerals and resistant phases, reflecting their low mobility and long-term geochemical stability within the soil matrix.

Samples	Fe	Mn	Pb	Cu	Zn	Ni	Co	Cr	Cd
	(mg/Kg)	(mg/Kg)	(mg/Kg)	(mg/Kg)	(mg/Kg)	(mg/Kg)	(mg/Kg)	(mg/Kg)	(mg/Kg)
SQ 1	251.118	105.746	18.723	14.103	31.411	11.652	6.342	5.126	0.343
SQ 2	252.049	108.224	17.916	14.321	30.782	11.761	6.226	5.472	0.345
SQ 3	345.371	147.602	24.432	20.438	35.255	15.004	7.752	6.159	0.798
SQ 4	352.217	147.916	25.543	20.825	36.126	15.243	8.116	6.458	1.128
SQ 6	184.382	83.239	12.621	13.127	26.134	9.827	4.279	4.174	0.312
SQ7	186.641	84.043	12.584	13.312	26.187	10.022	4.853	4.956	0.331
SQ 8	262.248	115.741	19.251	14.329	31.732	12.021	6.349	5.765	0.372
SQ 10	201.508	75.148	11.016	12.503	22.101	8.217	4.251	4.329	0.314
SQ 11	205.421	77.713	11.172	13.008	23.061	8.734	4.584	4.457	0.325
SQ 12	216.142	85.062	11.729	13.543	27.658	10.964	5.866	4.586	0.337
SQ 13	217.618	84.927	11.972	13.729	27.851	11.492	5.982	8.148	0.421
SQ 14	250.354	106.109	18.649	15.021	30.496	12.035	6.264	5.228	0.432
SQ 15	353.506	150.084	25.791	22.129	37.022	15.232	8.335	6.784	1.147
SQ 16	253.127	107.732	18.069	16.011	32.029	12.022	6.016	5.822	0.441
SQ 17	184.783	85.106	11.967	12.938	25.867	10.112	5.241	5.013	0.437

ISSN No. 2454-6194 | DOI: 10.51584/IJRIAS |Volume XI Issue VI June 2026

Table 8b: Statistical summary of the heavy metals concentration in the sulfide/strongly bound phase (mg/kg). This table presents the minimum, maximum, and mean concentrations of metals strongly bound within sulfide and resistant mineral phases, indicating their low mobility and high geochemical stability.

Metal	Fe	Mn	Pb	Cu	Zn	Ni	Co	Cr	Cd
Min	184.382	75.148	11.016	12.503	22.101	8.217	4.251	4.174	0.312
Max	353.506	150.084	25.791	22.129	37.022	15.243	8.335	8.148	1.147
Mean	247.766	104.293	16.762	15.289	29.581	11.623	6.030	5.498	0.499

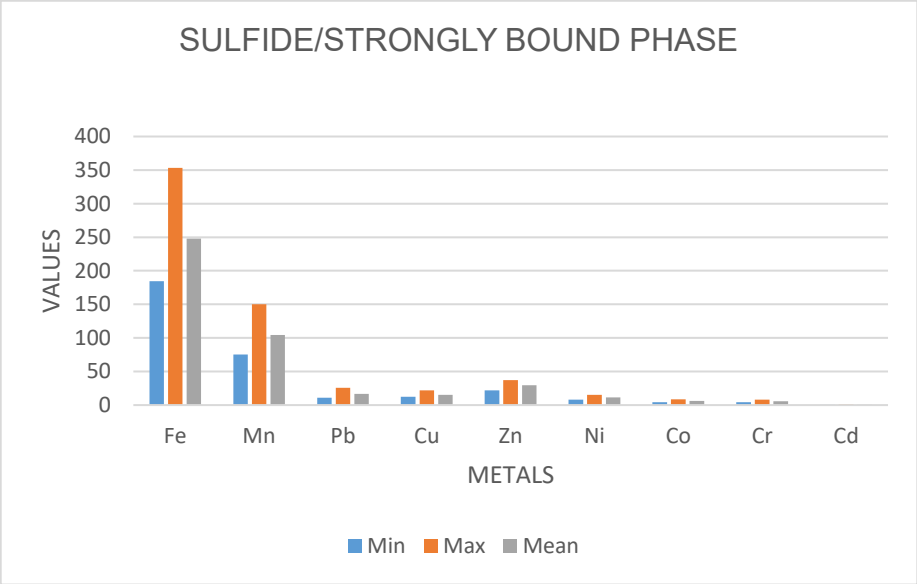

Figure 9. Cluster column chart of the heavy metal concentrations in the sulfide/strongly bound phase (mg/kg). The figure illustrates the distribution of metals strongly bound to sulfide and resistant mineral phases across all samples, highlighting their relative stability and low mobility in the geochemical system.

The Residual Phase

The residual phase represents metals strongly incorporated within primary and secondary mineral lattices (e.g., silicates, aluminosilicates, and resistant oxides), and it is widely regarded as the most stable and least mobile fraction in sequential extraction studies. Metals in this fraction are generally considered geochemically inert under normal environmental conditions and are only released through prolonged weathering or complete mineral breakdown (Tessier et al., 1979; Kabata-Pendias, 2011).

From **Table 9a**, Fe exhibits extremely high concentrations (12,532.459–16,416.143 mg/kg), confirming its dominance within primary silicate and ferromagnesian mineral structures. Mn (769.814–946.516 mg/kg) also shows strong lithogenic control, reflecting incorporation into silicate lattices and resistant oxide phases. Among trace metals, Zn (65.905–97.151 mg/kg) and Cu (51.031–62.631 mg/kg) occur at moderate levels, indicating structural substitution within aluminosilicate minerals. Pb (30.574–42.028 mg/kg) and Ni (29.364–43.833 mg/kg) similarly reflect lithogenic inheritance rather than secondary enrichment. Co (13.196–23.146 mg/kg) and Cr (55.704–80.015 mg/kg) are relatively elevated in this phase, consistent with their strong affinity for incorporation into mafic and ultramafic mineral structures. Cd remains very low (0.414–1.302 mg/kg), reflecting its limited structural incorporation and geochemical rarity in resistant mineral phases. The statistical summary **Table 9b** confirms the dominance order: Fe > Mn > Zn > Cr > Cu > Ni > Co > Pb > Cd, indicating strong lithogenic control and minimal influence of

ISSN No. 2454-6194 | DOI: 10.51584/IJRIAS |Volume XI Issue VI June 2026

secondary mobilization processes (Hakanson, (1980). . The narrow variability across samples further supports a uniform bedrock-derived geochemical signature.

Spatially, higher concentrations in SQ3, SQ4, SQ14, and SQ15 reflect zones enriched in ferromagnesian minerals or more mafic lithological influence, while relatively lower values in SQ6, SQ10, and SQ13 suggest more felsic or weathered lithologies. This spatial pattern is consistent with basement complex terrains where elemental distribution is primarily controlled by parent rock composition rather than anthropogenic inputs (Birth. (2003).

Figure 10 further confirms this interpretation, showing clear dominance of Fe and Mn across all samples, with other trace metals forming subordinate but stable distributions within the residual matrix. This reinforces the conclusion that most metals are locked within primary mineral structures and are not readily available for environmental mobilization.

Overall, the residual phase represents a long-term geochemical reservoir with negligible immediate environmental risk. However, it serves as a key indicator of bedrock composition and mineralogical control in the Ikole–Itapaji area, consistent with established sequential extraction frameworks in crystalline basement environments (Kabata-Pendias, 2011; Alloway, 2013).

Table 9a: Heavy metal concentrations in the residual phase (mg/kg). The table shows metals strongly locked within primary and secondary mineral lattices, representing the most stable and least mobile geochemical fraction in the soil system.

Samples	Fe	Mn	Pb	Cu	Zn	Ni	Co	Cr	Cd
	(mg/Kg)	(mg/Kg)	(mg/Kg)	(mg/Kg)	**(mg/Kg)**	(mg/Kg)	(mg/Kg)	(mg/Kg)	(mg/Kg)
SQ 1	13124.153	851.125	37.231	51.609	86.332	31.861	18.715	66.322	0.597
SQ 2	13231.582	862.197	35.793	52.096	84.809	32.168	19.207	66.188	0.553
SQ 3	16265.625	946.516	40.714	62.631	95.119	42.732	23.061	78.751	1.177
SQ 4	16416.143	941.849	42.028	61.979	97.151	43.833	23.146	80.015	1.185
SQ 6	15693.198	874.034	38.624	56.235	93.009	40.635	21.081	72.231	0.682
SQ7	12758.903	780.623	32.627	53.018	66.745	30.561	13.196	57.592	0.414
SQ 8	14753.727	865.106	36.942	54.723	88.126	34.642	20.731	68.685	1.127
SQ 10	12593.684	789.702	30.574	51.052	65.905	29.364	14.211	55.885	0.534

SQ 11	12682.363	776.937	31.077	51.031	68.016	29.902	13.723	55.759	0.511
SQ 12	14723.794	867.369	38.362	56.387	86.972	34.558	20.148	69.101	0.746
SQ 13	12532.459	769.814	30.984	52.125	68.132	32.092	13.741	55.704	0.642
SQ 14	15562.525	876.614	39.072	58.521	90.165	38.965	22.094	73.672	0.779
SQ 15	15469.538	872.607	40.729	57.985	92.007	39.018	21.628	71.961	1.302
SQ 16	13063.523	856.735	35.071	53.081	84.717	35.109	18.591	67.412	0.698
SQ 17	13274.221	842.699	34.866	52.983	85.458	35.238	18.793	66.923	0.602

Table 9b: Statistical summary of heavy metals in the residual phase (mg/kg). This table presents the minimum, maximum, and mean concentrations of metals retained in the residual fraction, representing the most stable and structurally bound geochemical pool in the soil matrix.

Metal	**Fe**	**Mn**	**Pb**	**Cu**	**Zn**	**Ni**	**Co**	**Cr**	**Cd**
Min	12532.459	769.814	30.574	51.031	65.905	29.364	13.196	55.704	0.414
Max	16416.143	946.516	42.028	62.631	97.151	43.833	23.146	80.015	1.302
Mean	14143.029	851.595	36.313	55.030	83.511	35.379	18.804	67.080	0.770

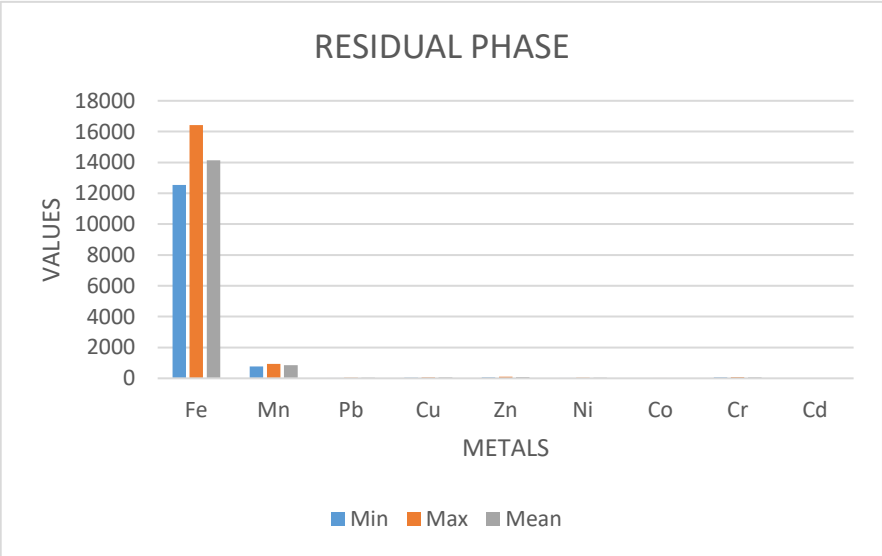

Figure 10. Cluster column chart of the heavy metal concentrations in the residual phase (mg/kg). The figure illustrates the distribution of metals in the residual fraction, highlighting their strong lithogenic control and dominance within primary mineral structures across all samples.

ISSN No. 2454-6194 | DOI: 10.51584/IJRIAS |Volume XI Issue VI June 2026

Contamination factor (CF) of Heavy Metals in Soils of the Study Area

According to the Contamination Factor (CF) values in **Table 10**, soils across the study area show varying degrees of heavy metal enrichment, reflecting both lithological influence and anthropogenic input. **Figure 11** illustrates these spatial trends across the 17 sampling stations (SQ1–SQ17), indicating clear variability in metal accumulation. Such patterns are typical of basement complex environments where natural weathering interacts with human activities (Reimann & de Caritat, 2005).

1. **Pollution Intensity and Spatial Distribution**

   Figure 11 shows that Cadmium (Cd) and Lead (Pb) dominate the pollution profile. Cd records the highest CF values, with severe contamination at SQ4 (6.08), SQ15 (6.20), and SQ3 (5.92), indicating significant enrichment. Pb also shows widespread contamination, with CF values between 2.42 and 4.20, reflecting considerable pollution across most locations.

2. **Geological Influence.**

   Comparison with the geological map shows that samples from Migmatite (Mg) and Gneiss (GG) zones, particularly around SQ1, SQ2, and SQ15, exhibit higher Cd levels. While basement lithology contributes to background metal content, the elevated CF values suggest additional enrichment beyond natural weathering processes (Reimann & de Caritat, 2005).

3. **Anthropogenic Influence and Summary**

   Higher Pb and Cu concentrations near settlements such as Ikole and Itapaji suggest anthropogenic inputs from agriculture and human activities. This aligns with the established understanding of metal mobility and partitioning in soils (Tessier et al., 1979; Förstner & Wittmann, 2012). Overall, the results indicate moderate to severe contamination dominated by Cd and Pb, with Fe showing minimal contamination and largely natural control.

Table 10. Contamination factor (CF) of heavy metals in soils of the study area, indicating the degree of metal enrichment relative to background concentrations and providing an assessment of the level of soil contamination across the sampled locations**.**

Sample	Fe	Mn	Pb	Cu	Zn	Ni	Co	Cr	Cd
SQ1	0.315	1.34	3.29	2.13	2.04	1.06	1.17	0.88	3.31
SQ2	0.318	1.37	3.20	2.17	2.02	1.09	1.19	0.91	3.17
SQ3	0.396	1.67	4.03	2.64	2.38	1.29	1.39	1.17	5.92
SQ4	0.401	1.68	4.20	2.67	2.43	1.35	1.42	1.21	6.08
SQ6	0.324	1.33	3.38	2.25	2.22	1.17	1.13	1.01	3.79
SQ7	0.290	1.18	2.82	2.02	1.85	0.97	0.92	0.83	2.68
SQ8	0.351	1.47	3.66	2.31	2.23	1.18	1.22	1.09	5.03
SQ10	0.273	1.06	2.42	1.73	1.57	0.86	0.74	0.76	2.21

ISSN No. 2454-6194 | DOI: 10.51584/IJRIAS |Volume XI Issue VI June 2026

SQ11	0.281	1.10	2.57	1.84	1.66	0.91	0.81	0.79	2.36
SQ12	0.338	1.34	3.41	2.22	2.19	1.14	1.13	1.03	3.88
SQ13	0.339	1.33	3.39	2.23	2.23	1.16	1.11	1.08	4.05
SQ14	0.372	1.60	3.73	2.46	2.33	1.24	1.20	1.13	4.32
SQ15	0.395	1.71	4.10	2.61	2.41	1.31	1.21	1.22	6.20
SQ16	0.342	1.36	3.27	2.30	2.22	1.19	1.18	1.12	4.51
SQ17	0.319	1.29	3.18	2.19	2.17	1.16	1.17	1.10	4.36

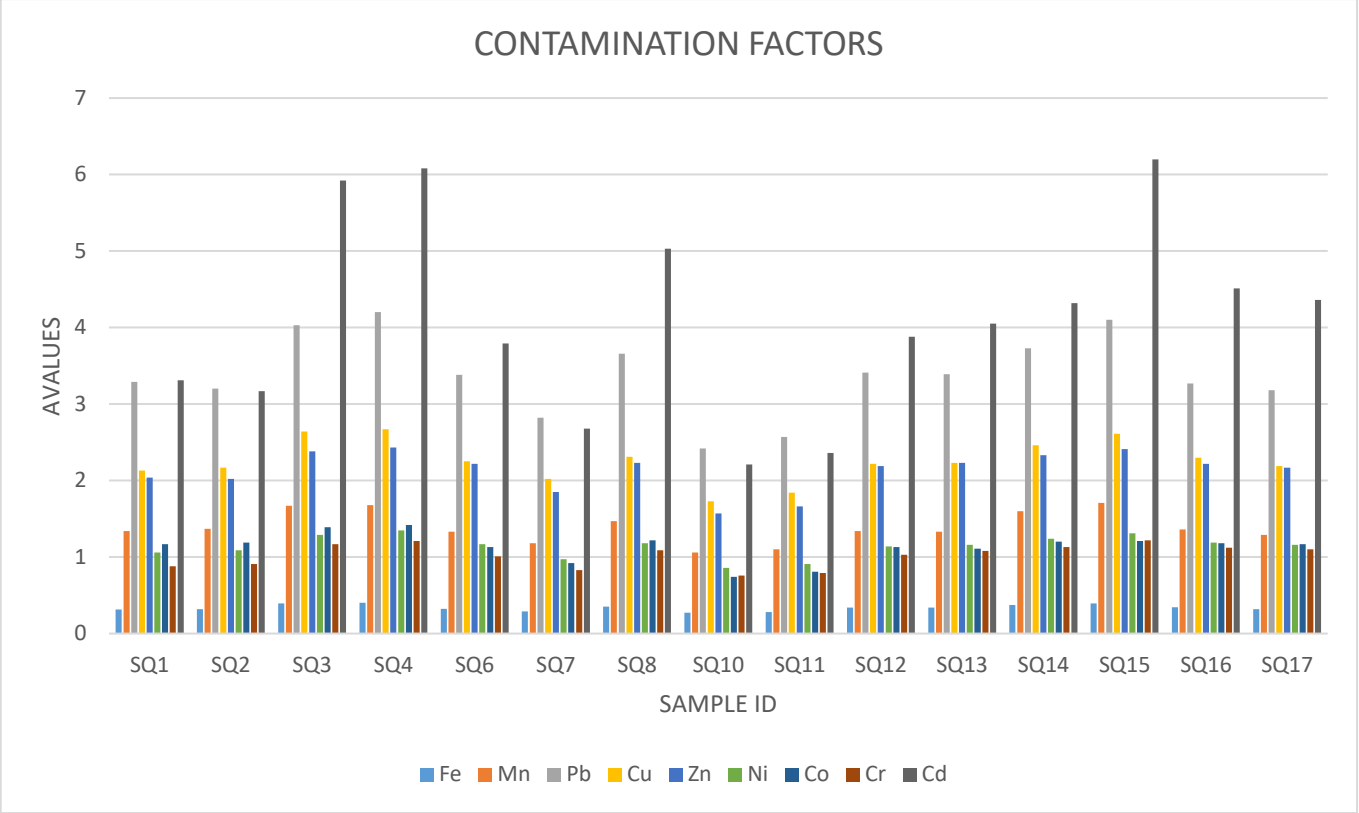

Figure 11: Clustered column chart showing the contamination factor of heavy metals in soil of the study area

Pollution Load Index (PLI) of Heavy Metals in Soils from the Study Area

The Pollution Load Index (PLI) provides an integrated assessment of overall heavy metal contamination by combining the contributions of all analyzed elements at each sampling location. From **Table 11 and Figure 12**, the spatial variation of soil quality across the study area can be effectively evaluated.

In general, the PLI interpretation follows the standard classification where PLI = 1 indicates baseline conditions, PLI > 1 reflects progressive soil deterioration due to pollution, and PLI < 1 suggests unpolluted or near-pristine conditions (Tessier et al., 1979; Förstner & Wittmann, 2012). Based on **Table 11**, most sampling points exhibit PLI values greater than 1, indicating widespread deterioration of soil quality and confirming the presence of significant heavy metal stress across the study area (Hakanson, (1980).

ISSN No. 2454-6194 | DOI: 10.51584/IJRIAS |Volume XI Issue VI June 2026

Spatially, **Figure 12** reveals distinct contamination hotspots, with the highest PLI values recorded at SQ15 (1.45), SQ4 (1.41), and SQ3 (1.38). These locations coincide with areas of more intense human activity and possible lithological influence from Migmatite–Gneiss transitions, which may enhance metal retention and accumulation (Reimann & de Caritat, 2005). In contrast, lower PLI values at SQ9 (0.85), SQ10 (0.86), and SQ11 (0.90) suggest relatively unpolluted conditions, likely reflecting reduced anthropogenic disturbance or more effective natural dispersion mechanisms.

The combined interpretation of **Table 11 and Figure 12** shows that soil contamination in the study area is spatially variable but generally elevated, with clear evidence of localized hotspots. This pattern reflects the combined influence of geogenic background variability and anthropogenic inputs, consistent with established soil geochemical behavior in complex terrains (Reimann & de Caritat, 2005; Förstner & Wittmann, 2012).

Table 11. Pollution Load Index (PLI) of heavy metals in soils from the study area, providing an integrated assessment of the overall level of soil contamination based on the combined contribution of all analyzed heavy metals across the sampled locations.

Sample	PLI
SQ1	1.12
SQ2	1.11
SQ3	1.38
SQ4	1.41
SQ6	1.15
SQ7	0.98
SQ8	1.27
SQ9	0.85
SQ10	0.86
SQ11	0.90
SQ12	1.18
SQ13	1.20
SQ14	1.31
SQ15	1.45
SQ16	1.29
SQ17	1.22

ISSN No. 2454-6194 | DOI: 10.51584/IJRIAS |Volume XI Issue VI June 2026

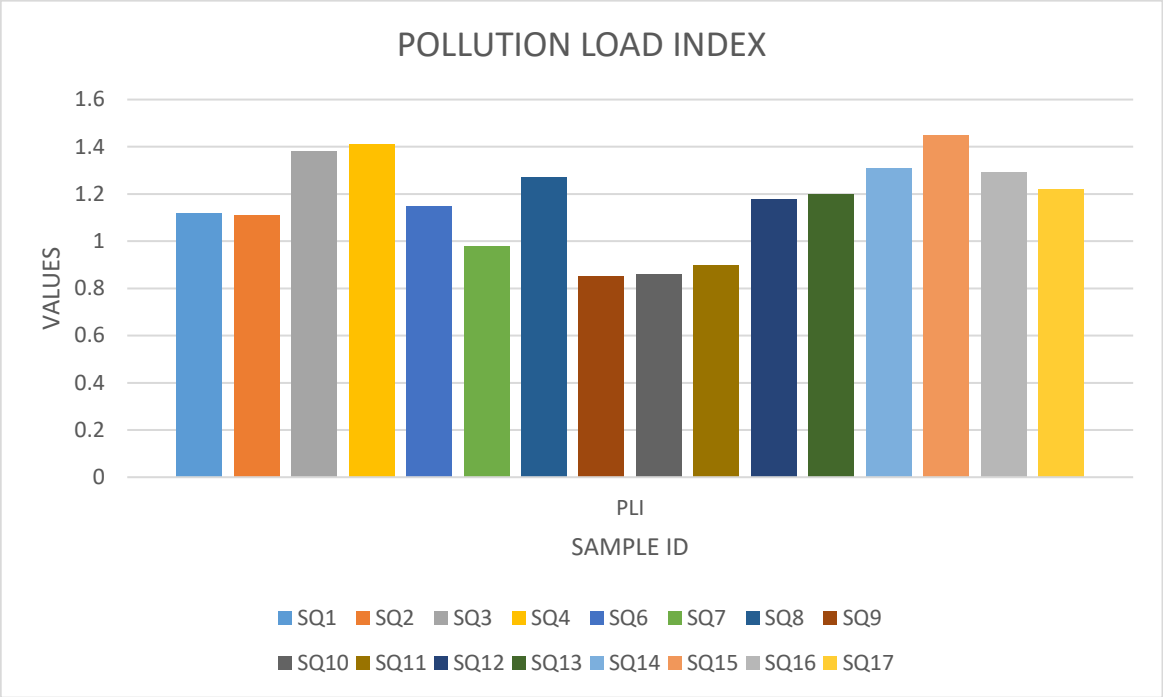

Figure 12: Clustered column chart showing the pollution load index of heavy metals in soil of the study area.

CONCLUSION

The Contamination Factor (CF) and Pollution Load Index (PLI) results collectively indicate that soils in the Ikole–Itapaji area exhibit varying degrees of heavy metal enrichment, reflecting both natural geological background and localized anthropogenic inputs. The CF results show that Cd and Pb are the most significant contaminants, with Cd reaching severe contamination levels in several locations (notably SQ3, SQ4, and SQ15), while Pb consistently indicates considerable enrichment across most sampling points. Other metals such as Zn, Cu, and Mn show moderate contamination, whereas Fe, Ni, Co, and Cr generally reflect low to background levels, suggesting dominant lithogenic control for these elements. The PLI values further confirm overall soil quality deterioration across the study area, with most samples exceeding the critical threshold of 1.0. High PLI values at SQ3, SQ4, SQ14, and SQ15 indicate localized contamination hotspots, while lower values at SQ9–SQ11 suggest relatively unpolluted zones. The integrated interpretation of CF and PLI demonstrates that soil contamination in the study area is spatially variable but generally elevated, with Cd and Pb representing the principal environmental concerns. The pattern reflects a combined influence of bedrock geology and human activities, consistent with typical basement complex geochemical behavior.

RECOMMENDATIONS

Based on the findings of this study, it is recommended that regular environmental monitoring of soil heavy metal concentrations be conducted within the Ikole–Itapaji area, with particular attention to Cd and Pb, which show the highest levels of contamination. This is important to track potential increases in metal accumulation and to prevent long-term ecological and human health risks.

Agricultural activities in identified hotspot areas (especially SQ3, SQ4, SQ14, and SQ15) should be carefully managed. The use of phosphate-based fertilizers, pesticides, and other agrochemicals should be regulated, as they may contribute to the observed enrichment of certain heavy metals, particularly Pb, Zn, and Cd. Farmers should also be encouraged to adopt soil management practices that reduce metal uptake, such as organic amendments and soil pH control.

It is further recommended that groundwater and surface water within the study area be analyzed for heavy metal contamination, since mobile fractions of metals may migrate from soils into water systems over time. This will help establish a more complete environmental risk profile.

Finally, environmental awareness programs should be introduced for local residents and stakeholders to promote safe land-use practices and reduce anthropogenic contributions to soil contamination.

LIMITATIONS OF THE STUDY

This study is limited by its focus on selected heavy metals and specific geochemical fractions, which may not fully capture the complete spectrum of contaminants present in the study area. Other potentially important elements or emerging contaminants were not included in the analysis.

The sequential extraction method used, while widely accepted, is operationally defined and may introduce some degree of phase overlap between fractions, which can affect absolute accuracy of metal partitioning results.

In addition, seasonal variations were not considered in the sampling design. Soil moisture, temperature, and redox conditions may influence metal mobility and could lead to temporal variations in contamination levels that were not captured in this study.

Finally, the study is limited to surface and near-surface soils, and does not account for deeper subsurface geochemical processes that may also influence metal distribution in the study area.

Availability of Data and Materials
The datasets used and analyzed during this study are available from the corresponding author upon reasonable request.

Disclaimer (Artificial Intelligence)
During the preparation of this work, the authors used ChatGPT (GPT-5-mini) to assist with language editing and content organization. After using this tool, the authors reviewed, revised, and verified all content to ensure accuracy, originality, and authenticity, and take full responsibility for the content of the published article.

Competing Interests

The authors have declared that no competing interests exist.

Authors' Contributions

Adeleke Ojo contributed to the conceptualization and design of the study, field sampling, laboratory analysis, data interpretation, and preparation of the initial manuscript draft. **Olusola Amos Olaolorun** was involved in the supervision of the research work, methodological review, interpretation of geochemical results, and critical revision of the manuscript for important intellectual content. **AKINOLA Oluwatoyin Olagoke** contributed to data processing, statistical and geochemical analysis, literature review, and editing of the final manuscript. All authors read and approved the final version of the manuscript.

REFERENCES

1. Abule, E. C., & Ekpete, O. A. (2025). Geochemical speciation and environmental implications of heavy metal mobility. https://doi.org/10.63561/fnas-jsi.v6i3.955
2. Çelebi, E. E. (2024). Determination of metal fractions and rare earth anomalies in red mud—Environmental Earth Sciences. https://doi.org/10.1007/s12665-023-11409-w
3. De Matteis, C., et al. (2023). Sequential extraction procedure in environmental studies. Frontiers in Environmental Science. https://doi.org/10.3389/fenvs.2023.1254205
4. Delina, R. E. G. (2024). Partitioning and mobility of chromium using sequential extraction. Environmental Science &Technology.

5. https://doi.org/10.1021/acs.est.3c10774
6. Firmino, F. H. T., et al. (2025). Efficiency of sequential extraction schemes in partitioning toxic elements. European Journal of Soil Science. https://doi.org/10.1111/ejss.70090
7. Ibrahim, R., et al. (2024). Sequential extraction of heavy metals in soils. https://doi.org/10.33003/fjs-2024-0803-2451
8. Ojo, O. F., Osazuwa, B. I., Chiemeke, C. C., Osumeje, O. J., Oyedele, A. A., Adagunodo, T. A., Oyeyemi, K. D., & Ejiga, E. G. (2024). Classification of the basement complex using aeromagnetic and remote sensing data analyses: Case study of Ekiti State, southwestern Nigeria. Earth Sciences Malaysia, 8(2), 158–162. https://doi.org/10.26480/esmy.02.2024.158.162
9. Adetunla, F. R., Ayodele, O. S., Asowata, I. T., & Olususi, J. (2025). Integrated geological, aeromagnetic and remote sensing datasets in litho-structural mapping of basement rocks in southwestern Nigeria. Asian Journal of Geological Research, 8(3), 523–553. https://doi.org/10.9734/ajoger/2025/v8i3213
10. Ogah, A. J., & Abubakar, F. (2024). Solid mineral potential evaluation using integrated aeromagnetic and aeroradiometric datasets. Scientific Reports, 14, 1637. https://doi.org/10.1038/s41598-024-52270-6
11. Salako, K. A., Adetona, A. A., Rafiu, A. A., Augie, A. I., Jimoh, M. O., Alkali, A., Muriana, R. A., & Lawrence, J. O. (2024). Integrated geophysical investigation for gold mineralization potential over the southern parts of Kebbi State, northwestern Nigeria. Heliyon, 10(14), e34093. https://doi.org/10.1016/j.heliyon.2024.e34093
12. Oyinloye, A. O. (2011). Geology and geotectonic setting of the basement complex rocks in Southwestern Nigeria: Implications on provenance and evolution. DOI: https://doi.org/10.5772/26990
13. Hakanson, L. (1980). An ecological risk index for aquatic pollution control: A sedimentological approach. Water Research, 14(8), 975–1001. https://doi.org/10.1016/0043-1354(80)90143-8
14. Rahaman, M. A. (1988). Recent Advances in the Study of the Basement Complex of Nigeria. In Precambrian Geology of Nigeria, Geological Survey of Nigeria, Kaduna, pp. 11–41. https://www.scirp.org/reference/referencespapers?referenceid=1712445
15. Nigerian Geological Survey Agency (NGSA), 2006. Geophysical mapping of Nigeria: Airborne radiometric and magnetic survey data, 2006. Available at: https://ngsa.gov.ng
16. Bouazizi, N., Baraud, F., Lemoine, M., & Leleyter, L. (2023). Shortened sequential extraction procedure: An effective and time-saving determination of trace metals in sediments. Soil and Sediment Contamination. DOI: https://doi.org/10.1080/15320383.2023.2293879
17. De Matteis, C., Mantovani, L., Tribaudino, M., et al. (2023). Sequential extraction procedure of municipal solid waste incineration bottom ash targeting grain size and amorphous fraction. Frontiers in Environmental Science, 11, 1254205. DOI: https://doi.org/10.3389/fenvs.2023.1254205
18. Doi, T., Hamasaki, S., Yamamoto, H., et al. (2023). Dynamic sequential extraction procedure for extracting mercury from soil samples. Analytical Sciences, 39(5), 739–748. DOI: https://doi.org/10.1007/s44211-023-00313-9
19. Çelebi, E. E. (2024). Determination of metal fractions and rare earth anomalies using modified sequential extraction. Environmental Earth Sciences, 83, 93. https://doi.org/10.1007/s12665-023-11409-w
20. Souza, J. P. R., Garnier, J., Quintarelli, J. M., et al. (2024). Adapted sequential extraction protocol for mercury speciation in mining environments. Toxics, 12(5), 326. https://doi.org/10.3390/toxics12050326
21. Bouazizi, N., Baraud, F., Lemoine, M., & Leleyter, L. (2023). Shortened sequential extraction procedure: An effective and time-saving determination of trace metals in sediments. Soil and Sediment Contamination. https://doi.org/10.1080/15320383.2023.2293879

22. Kabata-Pendias, A. (2011). Trace Elements in Soils and Plants (4th ed.). CRC Press. https://doi.org/10.1201/b10158
23. Reimann, C., & de Caritat, P. (2012). Chemical Elements in the Environment: Factsheets for the Geochemist and Environmental Scientist. Springer. DOI (https://doi.org/10.1007/978-3-642-72016-1 Publisher page: https://link.springer.com/book/10.1007/978-3-642-72016-1
24. Alloway, B. J. (2013). Heavy Metals in Soils: Trace Metals and Metalloids in Soils and their Bioavailability (3rd ed.). Springer. DOI: https://doi.org/10.1007/978-94-007-4470-7
25. Birth, G. (2003). A scheme for assessing human impacts on coastal aquatic environments using sediments. DOI: https://doi.org/10.1007/978-3-662-05950-8_7
26. Filgueiras, A. V., Lavilla, I., & Bendicho, C. (2002). Chemical sequential extraction for metal partitioning in environmental solid samples. Journal of Environmental Monitoring, 4, 823–857. DOI: https://doi.org/10.1039/B207574C
27. Förstner, U., & Wittmann, G. T. W. (2012). Metal Pollution in the Aquatic Environment. Springer. DOI: https://doi.org/10.1007/978-3-642-69385-4
28. Kabata-Pendias, A. (2011). Trace Elements in Soils and Plants (4th ed.). CRC Press. DOI: https://doi.org/10.1201/b10158
29. Reimann, C., & de Caritat, P. (2005). Distinguishing between natural and anthropogenic sources for elements in the environment. Science of the Total Environment, 337, 91–107. DOI: https://doi.org/10.1016/j.scitotenv.2004.06.011
30. Tessier, A., Campbell, P. G. C., & Bisson, M. (1979). Sequential extraction procedure for the speciation of particulate trace metals. Analytical Chemistry, 51, 844–851. DOI: https://doi.org/10.1021/ac50043a017
31. Kaiser, K., & Kalbitz, K. (2012). Cycling downwards – dissolved organic matter in soils. Soil Biology and Biochemistry, 52, 29–32. https://doi.org/10.1016/j.soilbio.2012.04.002
32. Liu, J., et al. (2022). Speciation of heavy metals in soils and their immobilization at micro-scale interfaces among soil components. Science of the Total Environment, 825, 153862. https://doi.org/10.1016/j.scitotenv.2022.153862
33. Davidson, C. M., Duncan, A. L., Littlejohn, D., Ure, A. M., & Garden, L. M. (1998). A critical evaluation of the three-stage BCR sequential extraction procedure to assess the potential mobility and toxicity of heavy metals in industrially-contaminated land. Analytica Chimica Acta, 363(1–2), 45–55. https://doi.org/10.1016/S0003-2670(98)00057-9
34. Wei, B., & Yang, L. (2010). A review of heavy metal contaminations in urban soils, urban road dusts and agricultural soils from China. Microchemical Journal, 94(2), 99–107. https://doi.org/10.1016/j.microc.2009.09.014
35. Adriano, D. C. (2001). Trace Elements in Terrestrial Environments: Biogeochemistry, Bioavailability, and Risks of Metals. Springer, New York. https://link.springer.com/book/10.1007/978-0-387-21510-5
36. Turekian, K. K., & Wedepohl, K. H. (1961). Distribution of the elements in some major units of the Earth's crust. Geological Society of America Bulletin, 72(2), 175–192. https://doi.org/10.1130/0016-7606(1961)72[175:DOTEIS]2.0.CO;2
37. Müller, G. (1969). Index of geoaccumulation in sediments of the Rhine River. GeoJournal, 2(3), 108–118. https://www.semanticscholar.org/paper/INDEX-OF-GEOACCUMULATION-IN-SEDIMENTS-OF-THE-RHINE-Muller/03688e2c0b4cabea9023db05e6b9a33281f0ea06